Korean Chem. Eng. Res., 57(5), 723-729 (2019)
https://doi.org/10.9713/kcer.2019.57.5.723
PISSN 0304-128X, EISSN 2233-9558

Onset of Buoyancy-Driven Convection in a Fluid-Saturated Porous Layer Bounded by Semi-infinite Coaxial Cylinders

Min Chan Kim†

Department of Chemical Engineering, Jeju National University, 102, Jejudaehak-ro, Jeju-si, Jeju-do, 63243, Korea
(Received 25 June 2019; Received in revised form 19 July 2019; accepted 22 July 2019)

Abstract – A theoretical analysis was conducted of convective instability driven by buoyancy forces under transient temperature fields in an annular porous medium bounded by coaxial vertical cylinders. Darcy's law and Boussinesq approximation are used to explain the characteristics of fluid motion and linear stability theory is employed to predict the onset of buoyancy-driven motion. The linear stability equations are derived in a global domain, and then cast into in a self-similar domain. Using a spectral expansion method, the stability equations are reformed as a system of ordinary differential equations and solved analytically and numerically. The critical Darcy-Rayleigh number is founded as a function of the radius ratio. Also, the onset time and corresponding wavelength are obtained for the various cases. The critical time becomes smaller with increasing the Darcy-Rayleigh number and follows the asymptotic relation derived in the infinite horizontal porous layer.

Key words: Stability, Porous medium, Buoyancy-driven convection, Coaxial cylinder

1. Introduction

The onset of buoyancy-driven motion in a horizontal porous layer begins with Horton-Rogers-Lapwood convection [1,2]. In a horizontal porous layer of infinite extent, all horizontal wave numbers are allowed. The critical wavenumber at the onset of convection determines the preferred convection cell. Later, Wooding [3] analyzed the onset condition of buoyancy-driven motion in a long vertical cylinder. In the cylindrical coordinate system, the convective structure in the horizontal plane is expressed in terms of Bessel functions in the radial direction. Later, Beck [4] generalized the Horton-Rogers-Lapwood problem to a finite rectangular box but assumed thermally insulating and impermeable lateral walls. In this case the pure Fourier modes persist as the horizontal eigenfunctions. Zebib [5], and Bau and Torrance [6] reconsidered this problem in the domains bounded by a finite circular cylinder or finite coaxial cylinders, respectively. For the system bounded by perfectly conducting walls, Haugen and Tyvand [7] analyzed the onset of convection in a porous medium bounded by a vertical cylinder. For the various geometries including coaxial cylinders, Rees and Tyvand [8] suggested eigenfunctions and the critical Rayleigh numbers. Later, Bringedal *et al*. [9] conducted linear and non-linear analyses on the onset of convection in a porous medium between coaxial cylinders. Barletta and Storesletten [10] revisited the onset of convection in a cylindrical porous medium by considering the heating from below and the cooling from above as caused by external forced convection processes.

The above mentioned work has been conducted on the onset of convection in a vertical porous cylinder under the linear density profile. However, most engineering applications relating to rapid changing of temperature and concentration fields involve a developing and nonlinear basic field. Therefore, it is important to predict when the buoyancy-driven motion sets in. Recently, the related stability analysis has been conducted in connection with CO_2 sequestration process. For the CO_2-sequestration system, Ennis-King *et al*. [11] were the pioneer researchers who studied the onset of buoyancy-driven convection systematically. Also, they considered the effect of the anisotropy of the porous medium on the onset of instability motion. Later, Riaz *et al*. [12] analyzed the onset of convection in a porous medium under the time-dependent concentration field in the similar coordinate. Kim and Choi [13] extended Riaz *et al*.'s analysis by considering the effect of the number of terms on the stability condition. Recently, for the infinite and semi-infinite cylinder system, Kim [14] and Myint and Firoozabadi [15] considered the lateral boundary effect on the onset of buoyancy-driven convection in a similar domain and global domain, respectively.

In the present study, the stability of initially quiescent, liquid-saturated, porous layer bounded by coaxial cylinders and heated from below is considered. Under the linear stability theory, stability equations are derived in the conventional global domain, and transformed in the self-similar one. To consider the effect of radial boundaries, the horizontal eigenmodes are expressed as the cylindrical harmonics. The critical conditions of the onset of buoyancy-driven convection are obtained by solving the resulting stability equations analytically and numerically. Since more complex geometry is considered in the present study, the effect of the lateral boundaries on the onset of

† To whom correspondence should be addressed.
E-mail: mckim@cheju.ac.kr

buoyancy driven convection is clearly explained.

2. Theoretical Analysis

2-1. Mathematical formulations

The system considered here is an initially quiescent, cylindrical porous layer saturated with liquid, as shown in Fig. 1. The solid substrate has a constant porosity ε and a constant permeability K. The interstitial fluid is characterized by the thermal expansion coefficient β, density ρ, heat capacity $(\rho c)_f$ and kinematic viscosity ν. The porous medium is regarded as a homogeneous and isotropic material with heat capacity $(\rho c)_e = \varepsilon(\rho c)_f + (1-\varepsilon)(\rho c)_s$ and thermal conductivity k_e. The effected thermal conductivity can be the weighted arithmetic mean, $k_e = \varepsilon k_f + (1-\varepsilon)k_s$, if the heat conduction in solid and fluid phases occurs in parallel, or the weighted geometric mean, $k_e = \varepsilon/k_f + (1-\varepsilon)/k_s$, if the heat conduction takes place in series. However, for practical purpose, the weighted geometric mean, $k_e = k_f^{\varepsilon} k_s^{(1-\varepsilon)}$, has been widely used [16]. Here subscripts *f* and *s* stand for fluid and solid substrate, respectively. Before heating, the fluid layer is maintained at uniform temperature T_i. For time $t \geq 0$ the lower boundary is suddenly heated with constant temperature T_b. Under the Boussinesq approximation, they can then be written as follows [3]:

$$\nabla \cdot \mathbf{U} = 0 \tag{1}$$

$$\frac{\mu}{K}\mathbf{U} = -\nabla P + \rho \mathbf{g} \tag{2}$$

$$\left(\frac{\partial}{\partial t} + \frac{(\rho c)_f}{(\rho c)^*}\mathbf{U}\cdot\nabla\right)T = \alpha_e \nabla^2 T \tag{3}$$

$$\rho = \rho_i\left[1-\beta(T-T_i)\right] \tag{4}$$

where $\mathbf{U}\left(=\mathbf{e}_r U + \mathbf{e}_\phi V + \mathbf{e}_z W\right)$ is the Darcy velocity vector in cylindrical $(\bar{r}, \phi, Z)$-coordinates, *T* the temperature, *P* the pressure, μ the viscosity, $\alpha_e\left(=k^*/(\rho c)^*\right)$ the effective thermal diffusivity, ρ_i the reference density, and **g** the gravitational acceleration It is assumed that the lateral wall is impermeable and perfectly insulating. The boundary conditions for the velocity and concentration fields are

$$\begin{aligned} &\frac{\partial W}{\partial r} = \frac{\partial T}{\partial r} = 0 \ \text{ at } \ \bar{r} = \eta R \text{ and } R, \\ &W = 0 \text{ and } T = T_b \text{ at } Z = 0, \\ &W = 0 \text{ and } T = T_i \text{ at } Z = \infty. \end{aligned} \tag{5}$$

The boundary conditions represent no radial mass and heat fluxes through the cylinder walls and fixed temperature on the lower and upper boundaries.

The important parameters to describe the present system are the Darcy-Rayleigh number Ra_D and radius ratio η defined by

$$Ra_D = \frac{g\beta K \Delta T R}{\alpha_e \nu}\frac{(\rho c)_f}{(\rho c)_e} \ \text{ and } \ \eta = \frac{R_i}{R} \tag{6}$$

where ν denotes the kinematic viscosity and $0 < \eta < 1$, i.e., $0 < R_i < R$. For the mass transfer system in a long vertical cylinder, Wooding [3] suggested the following critical condition of onset motion:

$$\frac{gKR^2}{D_e \mu}\left(\frac{d\rho}{dZ}\right) = 3.390\ , \tag{7}$$

where D_e is the effective mass diffusivity. Wooding [3] assumed that the density gradient is fully-developed and linear. For the case of infinite cylinder, however, the motion can be onset before the density profile is fully developed. Therefore, the stability problem becomes time dependent, and the critical time t_c and the minimum number to mark the onset of buoyancy-driven motion have practical importance. For this transient stability analysis we define a set of nondimensionalized variables τ, *z*, θ_0 by using the scale of time R^2/α_e, length *R* and temperature $\Delta T\left(=T_b - T_i\right)$. Then the basic conduction state is represented in dimensionless form of

$$\frac{\partial \theta_0}{\partial \tau} = \frac{\partial^2 \theta_0}{\partial z^2}\ , \tag{8}$$

with the following initial and boundary conditions,

$$\theta_0 = 0 \text{ at } \tau = 0, \tag{9a}$$

$$\theta_0 = 1 \text{ at } z = 0 \text{ and } \theta_0 \to 0 \text{ as } z = \infty. \tag{9b}$$

The above equations can be solved by using Laplace transform method as follows:

$$\theta_0 = \operatorname{erfc}\left(\frac{\zeta}{2}\right), \tag{10}$$

where $\zeta = z/\sqrt{\tau}$.

2-2. Stability equations

Under the linear stability theory, the disturbances caused by the onset of buoyancy-driven convection can be formulated, in dimensionless form, in terms of the temperature component c_1 and the vertical velocity component w_1 by decomposing Eqs. (1)-(3):

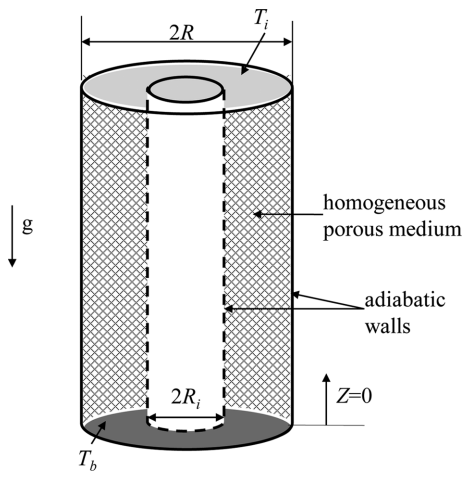

Fig. 1. Schematic diagram of the system considered here.

$$\nabla^2 w_1 = -\nabla_1^2 \theta_1 \tag{11}$$

$$\frac{\partial \theta_1}{\partial \tau} + Ra_D w_1 \frac{\partial \theta_0}{\partial z} = \nabla^2 \theta_1 \tag{12}$$

where $\nabla^2 = \frac{\partial^2}{\partial z^2} + \nabla_1^2$, $\nabla_1^2 = \frac{1}{r}\frac{\partial}{\partial r}\left(r\frac{\partial}{\partial r}\right) + \frac{1}{r^2}\frac{\partial^2}{\partial \phi^2}$ and $r = \bar{r}/R$. The velocity component has the scale of α_e / R and the concentration component has the scale of $\alpha_e \nu/(g\beta KR)$. The proper boundary conditions are given by

$$w_1 = \theta_1 = 0 \text{ at } z = 0 \text{ and } z = \infty \tag{13a}$$

$$\frac{\partial w_1}{\partial r} = \frac{\partial \theta_1}{\partial r} = 0 \text{ at } r = \eta \text{ and } 1. \tag{13b}$$

Now, the convective motion is assumed to exhibit the periodicity and the following Fourier mode analysis is employed:

$$[w_1, \theta_1] = \left[\bar{w}_1(\tau, z), \bar{\theta}_1(\tau, z)\right] X_l^m(r, \phi) \tag{14}$$

The cylindrical harmonics X_l^m satisfies the following relation [6]:

$$\nabla_1^2 X_l^m = -\alpha_{l,m}^2 X_l^m \tag{15a}$$

where

$$X_l^m(r, \phi) = \left\{A\, J_m(\alpha_{l,m} r) - B\, Y_m(\alpha_{l,m} r)\right\} \exp(im\phi),\ m = 0, 1, 2, \cdots \text{ and } l = 1, 2, \cdots \tag{15b}$$

and

$$J'_m(\alpha_{l,m}) Y'_m(\eta\alpha_{l,m}) - J'_m(\eta\alpha_{l,m}) Y'_m(\alpha_{l,m}) = 0,\ m = 0, 1, 2, \cdots \text{ and } l = 1, 2, \cdots. \tag{15c}$$

where $\alpha_{l,m}$ is the space wavenumber, and J_m and Y_m are the first and second kind Bessel function, respectively. The non-axisymmetric case of $m > 0$ satisfies the continuity requirement through the factor $\exp(im\theta)$. For the axi-symmetric case of $m = 0$, Eq. (15c) can be reduced as

$$J_1(\alpha_{l,0})\left\{Y_1(\eta\alpha_{l,0}) - Y_1(\alpha_{l,0})\right\} + Y_1(\alpha_{l,0})\left\{J_1(\alpha_{l,0}) - J_1(\eta\alpha_{l,0})\right\} = 0. \tag{16}$$

Also, the integral over the annulus cross section becomes

$$\int_\eta^1 r X_l^0(\alpha_{l,0} r)\, dr = \frac{1}{\alpha_{l,0}}\left[X_l^1(\alpha_{l,0}) - X_l^1(\eta\alpha_{l,0})\right]. \tag{17}$$

Through Eqs. (16) and (17), the continuity is satisfied even for the axi-symmetric modes.

Therefore, the stability equations are summarized as:

$$\left(\frac{\partial^2}{\partial z^2} - \alpha_{l,m}^2\right)\bar{w}_1 = \alpha_{l,m}^2 \bar{\theta}_1, \tag{18}$$

$$\frac{\partial \bar{\theta}_1}{\partial \tau} + Ra_D w_1 \frac{\partial \theta_0}{\partial z} = \left(\frac{\partial^2}{\partial z^2} - \alpha_{l,m}^2\right)\bar{\theta}_1. \tag{19}$$

under the following boundary conditions:

$$\bar{w}_1 = \bar{\theta}_1 = 0 \text{ at } z = 0 \text{ and } z = \infty, \tag{20}$$

Our goal is to find the critical time τ_c a given Ra_D and minimum Ra_D to mark the onset of convection for by using Eqs. (18)-(20).

Recently, Wessel-Berg [17] showed that the stability characteristics can be described more reasonably in the (τ, ζ)-domian rather than in the (τ, z)-one. In the (τ, ζ)-domian, it is natural that $\bar{\theta}_1(\tau, z) = \theta^*(\tau, \zeta)$ and $\bar{w}_1(\tau, z) = w^*(\tau, \zeta)$, where $\zeta(=\zeta/\sqrt{\tau})$ is the similarity variable introduced already in the base state of Eq. (10). Following a coordinate transformation to the similarity variable of ζ, the base state and the perturbation equations can be expressed as,

$$\left(D^2 - \alpha^{*2}\right) w^* = \alpha^{*2} \theta^*, \tag{21}$$

$$\tau\frac{\partial \theta^*}{\partial \tau} - \left(D^2 + \frac{\zeta}{2}D - \alpha^{*2}\right)\theta^* = Ra_D^* w^* D\theta_0, \tag{22}$$

with the following boundary conditions:

$$w^* = \theta^* = 0 \text{ at } \zeta = 0 \text{ and } \infty. \tag{23}$$

Here, $D = d/d\zeta$ $\alpha^* = \alpha_{l,m}\sqrt{\tau}$ and $Ra_D^* = RaD\sqrt{\tau}$ and $D\theta_0 = -\frac{1}{\sqrt{\pi}}\exp(-\zeta^2/4)$.

3. Solution Procedure

For the limiting case of $\tau \to 0$, i.e. $\alpha^* \to 0$ and $Ra_D^* \to 0$, the stability equations (21) and (22) can be rewritten as

$$D^2 w^* = 0, \tag{24}$$

$$\tau\frac{\partial \theta^*}{\partial \tau} = \left(D^2 + \frac{\zeta}{2}D\right)\theta^*, \tag{25}$$

The above equations are decoupled and the solution of Eq. (22) with boundary conditions (23) can be obtained as

$$w^* \to 0 \text{ as } \tau \to 0. \tag{26}$$

Since Eq. (25) is linear, the concentration disturbance can be expressed as

$$\theta^*(\tau, \zeta) = \sum_{i=1}^{\infty} a_i(\tau)\kappa_i f_i(\zeta), \tag{27}$$

where f_i is determined from the following Sturm-Liouville problem:

$$\left(D^2 + \frac{\zeta}{2}D\right) f_i = -\lambda_i f_i, \tag{28a}$$

under the following boundary conditions:

$$f_i = 0 \text{ at } \zeta = 0 \text{ and } \infty. \tag{28b}$$

The eigenfunction f_i and corresponding eigenvalue λ_i of the Sturm-Liouville Eq. (28) are

$$f_i = H_{2i-1}\left(\frac{\zeta}{2}\right)\exp\left(-\frac{\zeta^2}{4}\right) \text{ and } \lambda_i = i = 1, 2, \cdots \tag{29a\&b}$$

where $H_k(\xi)\left\{=(-1)^k \exp(\xi^2)\frac{d^k}{d\xi^k}\exp(-\xi^2)\right\}$ is the k-th Hermite polynomial. The scale factor

$\kappa_n = \left\{2^{n-1/2}\pi^{1/4}\sqrt{\Gamma(2n)}\right\}^{-1}$ is inserted to guarantee the orthonormal relation, i.e.

$$\kappa_m \kappa_n \int_0^\infty f_m f_n \exp\left(\frac{\zeta^2}{4}\right) d\zeta = \delta_{mn}, \tag{30}$$

where $\exp(\zeta^2/4)$ is the weighting function of the Sturm-Liouville equation (28).

By applying Eqs. (27)-(30) into Eq. (25), we can get the following amplitude equation:

$$\tau \frac{\partial a_i}{\partial \tau} = -\lambda_i a_i \quad \text{as } \tau \to 0. \tag{31}$$

The above relation means that for the limiting case of $\tau \to 0$, the following first mode is the most unstable disturbance:

$$\theta^*(\tau,\zeta) = a_1(\tau)\frac{1}{\sqrt{2\sqrt{\pi}}}\zeta \exp\left(-\frac{\zeta^2}{4}\right), \tag{32}$$

and its growth rate is

$$\sigma^*\left(=\frac{1}{a_1}\frac{da_1}{d\tau}\right) = -\frac{1}{\tau} \quad \text{as } \tau \to 0. \tag{33}$$

For the general time-evolving case, from Eqs. (21) and (27), w^* is expressed as

$$w^* = \sum_{i=1}^{\infty} a_i(\tau)\kappa_i g_i(k^*,\zeta), \tag{34}$$

where g_i can be obtained by solving

$$\left(D^2 - \alpha^{*2}\right) g_i = \alpha^{*2} f_i, \tag{35a}$$

under the following boundary conditions:

$$g_i = 0 \text{ at } \zeta = 0 \text{ and } \zeta \to \infty. \tag{35b}$$

Using the method of variation of parameters [17] or the inverse operator technique [13], the solutions of Eq. (35) can be expressed as

$$g_i = -\frac{\alpha^*}{2}\exp(-\alpha^*\zeta)\int_0^\zeta f_i \exp(\alpha^*\xi)d\xi + \frac{\alpha^*}{2}\exp(\alpha^*\zeta)\int_0^\zeta f_i \exp(-\alpha^*\xi)d\xi - \alpha^* \sinh(\alpha^*\zeta)\int_0^\infty f_i \exp(-\alpha^*\xi)d\xi \tag{36}$$

After performing the integrations, Eq. (36) can be simplified recursively as

$$g_i = 4\alpha^{*2}(g_{i-1} - f_{i-1}), \quad i = 2,3,\cdots \tag{37a}$$

with

$$g_1 = -\alpha^{*2}\sqrt{\pi}\exp(\alpha^{*2}) \left[\exp(-\alpha^*\zeta)\operatorname{erf}\left(-\alpha^* + \frac{\zeta}{2}\right) + \exp(\alpha^*\zeta)\operatorname{erf}\left(\alpha^* + \frac{\zeta}{2}\right) - 2\sinh(\alpha^*\zeta)\right] \tag{37b}$$

Substituting θ^* and w^* into Eq. (22) and performing the orthogonalization process, the stability equations are reduced to the following matrix form:

$$\tau \frac{d\mathbf{a}}{d\tau} = \mathbf{B}\mathbf{a}, \tag{38a}$$

where

$$B_{mn} = -\left(\lambda_m + \alpha^{*2}\right)\delta_{mn} + Ra_D^*\kappa_m\kappa_n C_{mn}, \tag{38b}$$

$$C_{mn}(\alpha^*) = \int_0^\infty f_m(\zeta) g_n(\alpha^*,\zeta) d\zeta, \tag{38c}$$

$$\mathbf{a} = [a_1, a_2, a_3, \cdots]^T, \tag{38d}$$

for m, $n = 1,2,\cdots$. It is stressed that the partial differential Eqs. (21)-(23) are reduced into the simultaneous ordinary differential Eqs. (38), without spatial discretization. Furthermore, the characteristic matrix $\mathbf{B}$ is normal, i.e. $\mathbf{B}=\mathbf{B}^T$, since $C_{mn} = C_{nm}$ through

$$C_{mn} = \int_0^\infty f_m g_n d\zeta = -\frac{1}{\alpha^{*2}}\int_0^\infty f_m\left(\frac{d^2}{d\zeta^2} - \alpha^{*2}\right) f_n d\zeta = \int_0^\infty \left(\frac{1}{\alpha^{*2}}\frac{df_m}{d\zeta}\frac{df_n}{d\zeta} + f_m g_n\right) d\zeta = C_{nm} \tag{39}$$

If the characteristic matrix $\mathbf{B}$ is normal, it is possible to set $d\mathbf{a}/d\tau = \sigma^*\mathbf{a}$ and therefore, Eq. (38a) can be reduced as [13]

$$\sigma^*\tau\mathbf{a} = \mathbf{B}\mathbf{a}. \tag{40}$$

Based on the above relation, the growth rate can be given as

$$\sigma^*\tau = \max\left[\operatorname{eig}(\mathbf{B})\right], \tag{41}$$

where $\max\left[\operatorname{eig}(\mathbf{B})\right]$ means the maximum eigenvalue of the matrix $\mathbf{B}$.

For the present normal system, it is possible to set $d\theta^*/d\tau = \sigma^*\theta^*$, which is equivalent to $d\mathbf{a}/d\tau = \sigma^*\mathbf{a}$, and therefore, stability Eqs. (21) and (22) can be reduced as

$$\left(D^2 - \alpha^{*2}\right) w^* = \alpha^{*2}\theta^*, \tag{21}$$

$$\sigma^*\tau\theta^* - \left(D^2 + \frac{\zeta}{2}D - \alpha^{*2}\right)\theta^* = Ra_D^* w^* D\theta_0, \tag{42}$$

Here, note that the above equations are derived without the quasi-steady state approximation (QSSA) and are slightly different from Robinson's [18] (see Robinson's equation (11) and (12)). In Robinson's [18] analysis, the $(\zeta/2)D\theta^*$-term in Eq. (42) is neglected and, therefore, his approach corresponds to the well-known frozen-time model.

The above stability Eqs. (21) and (42) are solved by employing the outward shooting scheme [19,20]. To obtain the growth rate σ^*, the proper values of w^* and $D\theta^*$at $\zeta = 0$ are assumed for given α^* and Ra_D^*. Since the stability equations and their boundary conditions are all homogeneous, the value of $w^*(0)$ can be assigned arbitrarily and the value of the parameter $\sigma^*\tau$ is assumed. This procedure can be understood easily by taking into account the characteristics of eigenvalue problems. After all the values at $\zeta = 0$ are provided, this eigenvalue problem can proceed numerically.

Integration is performed from $\zeta = 0$ to an arbitrary upper with the fourth-order Runge-Kutta-Gill method. If the guessed values of $\sigma^*\tau$ and $D\theta^*(0)$ are correct, w^* and θ^* will vanish at the upper boundary. To improve the initial guesses the Newton-Raphson iteration is used. For the present system, the position of the upper boundary is infinity. To consider the infinity boundary effect, the Shanks transformation is used.

4. Results and Discussion

The neutral stability condition can be determined by setting $\sigma^* = 0$. The neutral stability curves obtained from the numerical shooting method and the present analytical approximations are compared in Fig. 2. The leading-term analysis, which corresponds to the 1-term approximation, is also conducted and summarized in Fig. 2. As shown, for the limiting case of $\alpha^* \to 0$, all the methods produce nearly the same stability condition. However, with increasing α^*, the lower order approximations start to deviate from the numerical shooting solution. This figure shows that the 7-term approximation is sufficient enough to describe the neutral stability conditions. Using the 7-term approximation, the neutral stability curve is redrawn in the ($Ra_D\sqrt{\tau}$, α/Ra_D)-domain. This figure means that the disturbance having the wavenumber $\alpha/Ra_D > 0.101$ is unconditionally stable. By comparing the frozen time model based on the QSSA, the $(\zeta/2)D\theta^*$-term makes the system stable.

Unlike the horizontally unbounded system of infinite horizontal layer, the cylinder walls restrict the feasible wavenumber through Eq. (15c), that is, the wavenumber has discrete values. For the typical cases of η, the critical time for a given Ra_D and several smallest wavenumbers is summarized in Fig. 3. In this figure, for a given η, the preferred unstable modes are given as a function of Ra_D and η. Fig. 3(b) shows that for the typical case of $Ra_D = 30$, as time goes on, the initially stable system becomes unstable, and the preferred unstable mode becomes in the order of $\alpha_{2,1}$, $\alpha_{1,1}$, $\alpha_{2,1}$ and $\alpha_{1,1}$. Finally, the system becomes stable. Also, these figures show that the critical conditions obtained for the unbounded system can be approximately valid for $Ra_D > 100$.

As shown in this figure, non-axisymmetric mode of $\{J_1(\alpha_{1,1}r)/J_1'\alpha_{1,1} - Y_1(\alpha_{1,1}r)/Y_1'(\alpha_{1,1})\}\exp(i\theta)$ gives the most unstable mode and suggests the minimum Ra_D to induce the convective motion and $Ra_{D,c}$ can be calculated from

$$Ra_{D,c} = \frac{\alpha_{1,1}}{0.101}, \tag{43}$$

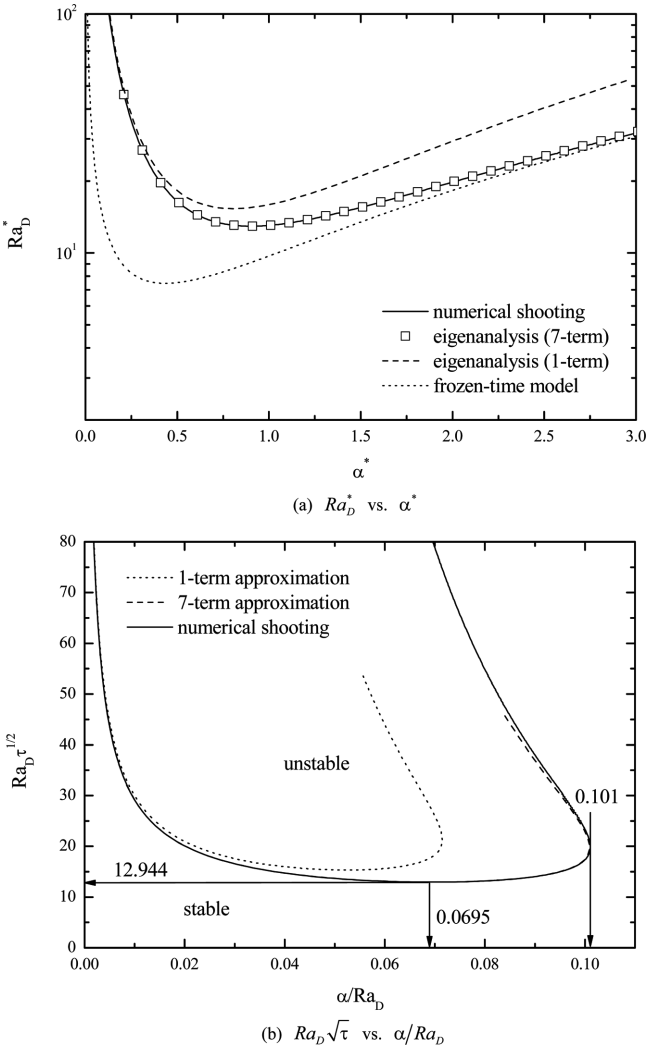

Fig. 2. Neutral stability curves for the various methods. (a) Ra_D^* vs. α^* and (b) $Ra_D\sqrt{\tau}$ vs. α/Ra_D.

where 0.101 is the maximum value of α/Ra_D for the unstable mode (see Fig. 2). The effect of annulus ratio on the critical Ra_D is summarized in Fig. 4. As shown, the system having a wide gap is more stable. This is opposite to the well-known fact that the lateral boundaries make the system stable.

The present critical condition, Eq. (43) is quite different from $Ra'_{D,c}\left\{=\frac{gKR^2}{\alpha_e\mu}\left(\frac{d\rho}{dZ}\right)\frac{(\rho c)_f}{(\rho c)_e}\right\} = \alpha_{1,1}^2$ of Wooding's [3] and Bau and Torrance's [6]. They assumed $\partial\rho/\partial Z\,(=\Delta\rho/L_c)$ is constant for a long cylinder, where L_c is the penetration depth. From the above two critical conditions, one may say that if $Ra_D > \alpha_{1,1}/0.101$, the system is unstable; however, as the instability motion develops, the density gradient becomes linear and the instability motion ceases when $Ra'_D < Ra'_{D,c}(=\alpha_{1,1}^2)$. $Ra_{D,c}$ is compared with the present $Ra_{D,c}$ in Fig. 4. This transition from the unstable state into the stable one was observed by Wooding [3]. In the mass transfer system, the transition condition can be used to determine the diffusivity by measuring the

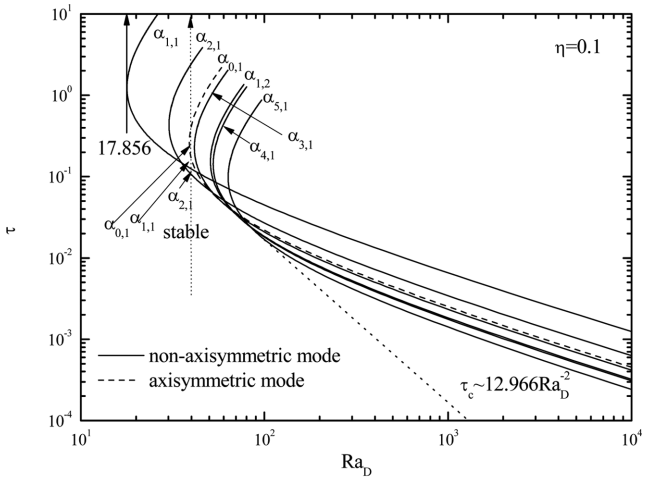

(a) $\eta = 0.1$

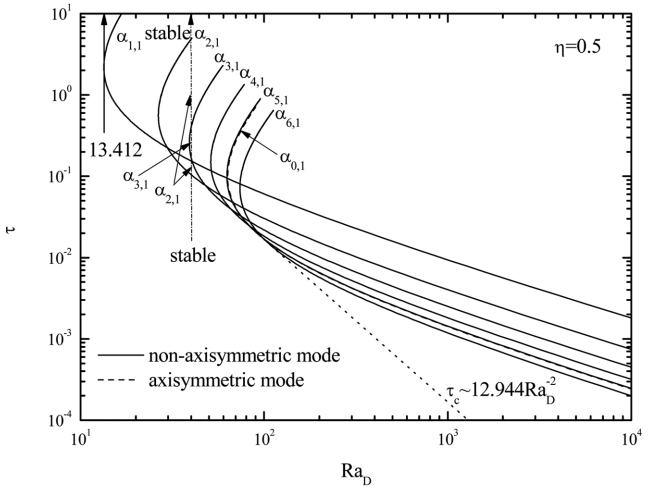

(b) $\eta = 0.5$

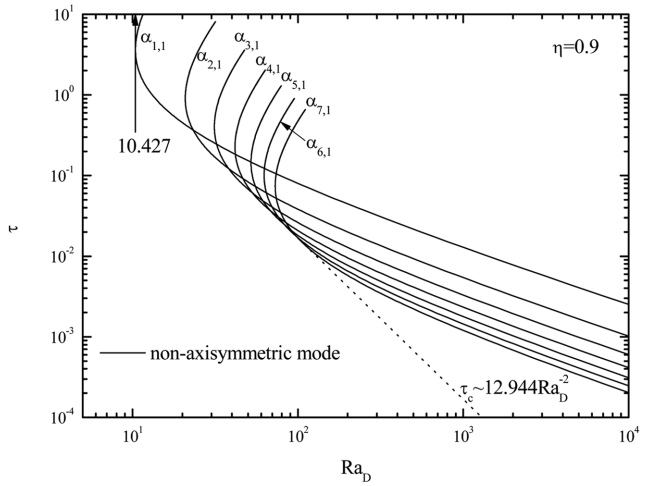

(c) $\eta = 0.9$

Fig. 3. Critical time from for the smallest seven wavenumbers for the cases of (a) η = 0.1, (b) η = 0.5 and (c) η = 0.9.

penetration depth at a condition of stability [21]. Based on Eq. (43), the diffusivity can be determined as

$$D_e = \frac{0.101}{\alpha_{1,1}} \frac{g\beta KR}{\nu(\Delta C)_c}, \tag{44}$$

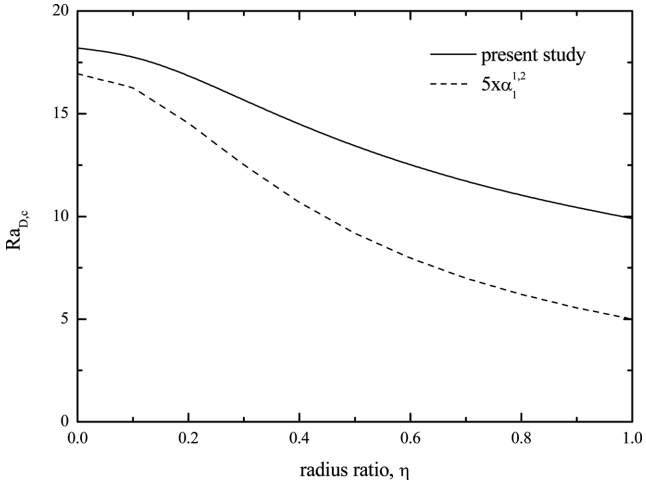

Fig. 4. Effect of the radius ratio on the critical Darcy-Rayleigh numbers.

where $(\Delta C)_c$ is the minimum concentration difference to ensure the onset of convective motion.

The critical time decrease with increasing Ra_D and if all the possible wavenumbers are superimposed, it follows the asymptotic relation of $\tau_c = (12.944/Ra_D)^2$, which is derived in the unbounded horizontal domain [13]. For high Ra_D the buoyancy-driven convection can be set in at small time, and therefore the buoyancy-driven instability is confined to the narrow region near the heated boundary. Therefore, radial boundary effects can be neglected, and the system can be considered an infinite horizontal layer. For the unbounded infinite horizontal layer, the minimum value of Ra_D^* and corresponding α^* in the Fig. 2 can be used to determine the critical condition marking the onset of buoyancy-driven convection. Regardless of the annulus ratio, the stability criteria can be expressed for the infinite horizontal system as follows:

$$t_c = 167.547\left(\frac{\nu\alpha_e^{1/2}}{g\beta K\Delta T}\frac{(\rho c)^*}{(\rho c)_f}\right)^2 \quad \text{and} \quad \lambda_c = 90.406\left(\frac{\nu\alpha_e}{g\beta K\Delta T}\frac{(\rho c)^*}{(\rho c)_f}\right)$$

$$Ra_D \gg Ra_{D,c} \tag{45}$$

5. Conclusions

The onset of buoyancy-driven motion in a fluid-saturated, cylindrical porous layer heated from below was analyzed theoretically by using linear stability theory. The critical Darcy-Rayleigh number and onset time of buoyancy driven motion for a given Darcy-Rayleigh number were determined as a function of the radius ratio. The present initial growth rate analysis shows that the system is unconditionally stable regardless of the radius ratio. The present analysis, without invoking the QSSA, predicts the onset time quite reasonably and the $(\zeta/2)R\theta^*$-term, which is ignored in the frozen-time model under the QSSA, makes the system more stable. The effect of the ratio of radius on the critical condition is important for the small Ra_D-case, however, for the Ra_D-system the onset time of the buoyancy deriven instability is

insensitive to the radius ratio.

Acknowledgments

This research was supported by the 2019 scientific promotion program funded by Jeju National University.

References

1. Horton, C. W. and Rogers, F. T., "Convection Currents in a Porous Medium," *J. Appl. Phys.,* **16**(6), 367(1945).
2. Lapwood, E. R., "Convection of a Fluid in a Porous Medium," *Proc. Camb. Phil. Soc.*, **44**(4), 508(1948).
3. Wooding, R. A., "The Stability of Viscous Liquid in a Vertical Tube Containing Porous Material," *Proc. Roy. Soc. London A* **252**(1268), 120(1959).
4. Beck, J. L., "Convection in a Box of Porous Material Saturated with Fluid," *Phys. Fluids* **15**(8), 1377(1972).
5. Zebib, A., "Onset of Natural Convection in a Cylinder of Water Saturated Porous Media," *Phys. Fluids* **21**(4), 699(1978).
6. Bau, H. H. and Torrance, K. E., "Onset of Convection in a Permeable Medium Between Vertical Coaxial Cylinders," *Phys. Fluids* **24**(3), 382(1981).
7. Haugen, K. B. and Tyvand, P. A., "Onset of Thermal Convection in a Vertical Porous Cylinder with Conducting Wall," *Phys. Fluids* **15**(9), 2661(2003).
8. Rees, D. A. and Tyvand, P. A., "The Helmholtz Equation for Convection in Two-dimensional Porous Cavities with Conducting Boundaries," *J. Eng. Math.* **49**(2), 181(2004).
9. Bringedal, C., Berre, I., Nordbotten, J. M. and Rees, D. A. S. "Linear and Nonlinear Convection in Porous Media Between Coaxial Cylinders," *Phys. Fluids* **23**(9), 094109(2011).
10. Barletta, A. and Storesletten, L., "Effect of a Finite External Heat Transfer Coefficient on the Darcy-Bénard Instability in a Vertical Porous Cylinder," *Phys. Fluids*, **25**(4), 044101(2013).
11. Ennis-King, J., Preston, I. and Paterson, L., "Onset of Convection in Anisotropic Porous Media Subject to a Rapid Change in Boundary Conditions," *Phys. Fluids* **17**(8), 084107(2005).
12. Riaz, A., Hesse, M., Tchelepi, H. A. and Orr, F. M., "Onset of Convection in a Gravitationally Unstable, Diffusive Boundary Layer in Porous Media," *J. Fluid. Mech.* **548**, 87(2006).
13. Kim, M. C. and Choi, C. K., "Linear Stability Analysis on the Onset of Buoyancy-driven Convection in Liquid-saturated Porous Medium," *Phys. Fluids* **24**(4), 044102(2012).
14. Kim, M. C., "Onset of Buoyancy-driven Convection in a Fluid Saturated Porous Layer Bounded by a Long Cylinder," *Trans. Porous Med.,* **97**(3), 395(2013).
15. Myint, P. C. and Firoozabadi, A., "Onset of Buoyancy-driven Convection in Cartesian and Cylindrical Geometries," *Phys. Fluids*, **25**(4), 044105(2013).
16. Nield, D. A. and Bejan, A., Convection in porous media. 3rd ed. Springer(2016).
17. Wessel-Berg, D., "On a Linear Stability Problem Related to Underground CO_2 Storage," *SIAM J Appl. Math.*, **70**(4), 1219 (2009).
18. Robinson, J. L., "Theoretical Analysis of Convective Instability of Growing Horizontal Thermal Boundary Layer," *Phys Fluids* **19**(6), 778(1976).
19. Ryoo, W. S. and Kim, M. C., "Effect of Vertically Varying Permeability on the Onset of Convection in a Porous Medium," *Korean J. Chem. Eng.*, **35**(6), 1247(2018).
20. Kim, M. C., "Energy Stability Analysis on the Onset of Buoyancy-driven Convection in a Horizontal Fluid Layer Subject to Evaporative Cooling," *Korean Chem. Eng. Res.*, **57**(1), 142(2019).
21. Southard, M. Z., Dias, L. J., Himmelstein, K. J. and Stella, V. J., "Experimental Determination of Diffusion Coefficients in Dilute Aqueous Solution Using the Method of Hydrodynamic Stability," *Pharmaceutical Res.*, **8**(12), 1489(1991).